PAPER • **OPEN ACCESS**

Quantifying phase transformation during the manufacturing process of AISI 430 ferritic stainless steel

To cite this article: I Collado *et al* 2020 *IOP Conf. Ser.: Mater. Sci. Eng.* **891** 012007

View the article online for updates and enhancements.

This content was downloaded from IP address 150.214.75.244 on 08/03/2021 at 07:33

IOP Conf. Series: Materials Science and Engineering **891** (2020) 012007 doi:10.1088/1757-899X/891/1/012007

Quantifying phase transformation during the manufacturing process of AISI 430 ferritic stainless steel

I Collado[1], A Núñez Galindo[2], A Ruiz[2], J F Almagro Bello[2] and F J Botana[1]

[1] Universidad de Cádiz, Escuela Superior Ingeniería, Departamento de Ciencia de los Materiales e Ingeniería Metalúrgica y Química Inorgánica, LABCYP Group, Avda. Universidad de Cádiz 10, 11519 Puerto Real, Spain
[2] Acerinox Europa S.A.U, Departamento Técnico / Laboratorios e Investigación, Pol. Industrial Palmones s/n, 11379 Los Barrios, Spain

E-mail: irene.collado@uca.es

Abstract. The effect of ferrite to austenite transformation phenomenon on microstructure and annealing performance of AISI 430 (EN 1.4016) ferritic stainless steel 16%Cr-0.04%C and 17%Cr-0.02%C was studied by electron backscatter diffraction and X-ray diffraction. Hot-rolled and annealed specimens of each ferritic stainless steel were collected from manufacturing route, where different states were analysed. Chemical composition shift of AISI 430 is correlated to microstructural behaviour of each material, while annealing temperature impact over grain growth phenomena is discussed.

1. Introduction

AISI 430 ferritic stainless steel is becoming highly demanded on cold-forming processes [1], such as household appliances and, in some applications, as a replacement of austenitic stainless steel [2]. Compered to austenitic stainless steel, which provides an outstanding metallurgical property, the absence or low content of nickel in AISI 430 results in an attractive economic solution for many applications. Therefore, the aim of metallurgical manufacturers involves the enhancement of surface quality and appearance of ferritic stainless steel finishing [3]. Surface defects related to AISI 430 ferritic stainless steel, are caused in many occasions by their structural complexity. This feature structure is related to the ferrite/austenite transformation that takes place within the ferritic matrix of this stainless steel, mostly, during hot rolling [4]. The critical temperature at which phase transformation takes place is described as A_{c1}, and depends on many factors, such as alloy chemical composition and annealing rate.

For that reason, annealing is a crucial production step. During this process, stainless steel is exposed to high temperatures below A_{c1} long enough for the whole austenite to ferrite + carbides transformation to take place. If this process is performed badly, ferritic matrix would retain austenite. Consequently, the remaining austenitic phase will turn into martensite when the steel reaches a certain temperature during cooling where martensitic phase starts to nucleate, also known as Ms temperature. During annealing, AISI 430 theoretically recover its ferritic mono-phase before ending this heat treatment. Moreover, after being the austenite completely transformed into ferrite, annealing process must ensure the re-crystallisation of the ferritic structure and, therefore, recuperate its mechanical property according to its composition.

Content from this work may be used under the terms of the Creative Commons Attribution 3.0 licence. Any further distribution of this work must maintain attribution to the author(s) and the title of the work, journal citation and DOI.
Published under licence by IOP Publishing Ltd

Overall, this research attempt to measure the remaining martensite as a clear indicator of the previous phase transformation by using AZTEC RECLASSIFY PHASE from electron backscatter diffraction (EBSD) and X-ray diffraction (XRD). At the same time, the microstructure of these materials is characterised during hot rolling and annealing. The study has been carried out forward comparative analysis of two sorts of AISI 430 ferritic stainless steel. One of these materials represents AISI 430 standard composition whereas compositional and manufacturing changes are assumed in the other.

2. Materials and experimental procedures

This work used two AISI 430 ferritic stainless steel compositions, whose samples were collected from hot rolling, annealing and pickling and bright annealing. Specifications of each specimen are listed in the Table 1, where stainless steel composition was analysed by X-ray fluorescence (XRF).

Table 1. Composition and characteristic of the samples collected from manufacturing process of flat stainless steel product. Eq_{Cr} was calculated by the Schaefler equation [5] (Eq_{Cr} = %Cr + %Mo + 1.5·%Si + 0.5·%Nb + 2·%Ti).

AISI 430	Composition, %	Eq_{Cr}	Measurement point (manufacturing)	Specimen thickness, mm
1A	16Cr 0.3Si 0.4Mn 0.045C 0.040N_2	11.3	Hot rolling Annealing and pickling Bright annealing	26 4 0.7
2A	17Cr 0.4Si 0.3Mn 0.020C 0.033N_2	13.2	Hot rolling Annealing and pickling Bright annealing	26 3.5 0.4

AISI 430 composition has slightly changed from 1A to 2A, where chromium, carbon and nitrogen shifts have a great impact on the ferrite - austenite transformation phenomenon, as shown in Fig 1.

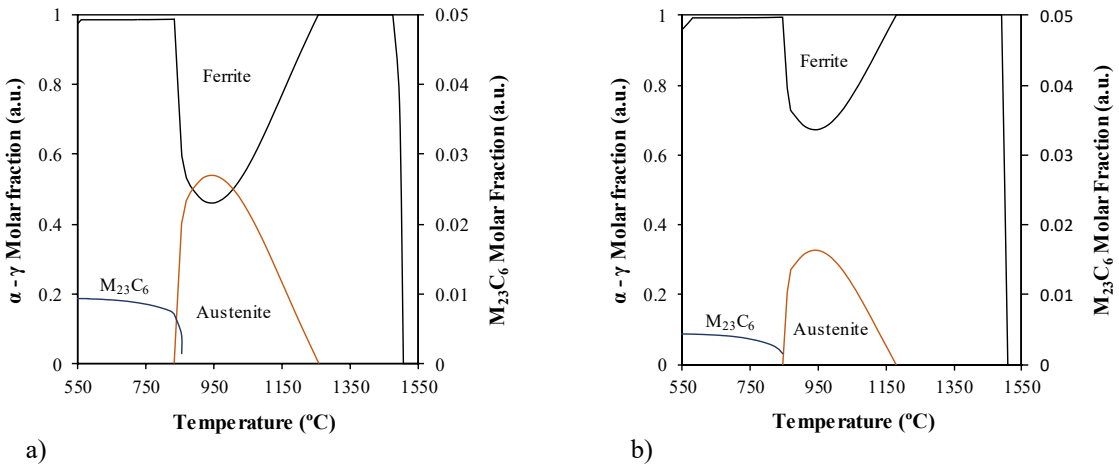

Figure 1. Molar fraction of phase transformation in equilibrium of AISI 430; a) material 1A, and b) material 2A, by THERMOCALC (TCW5) [6].

Moreover, Fig. 1 shows $M_{23}C_6$ precipitation, which is formed in the course of $\alpha \rightarrow \gamma + (Fe, Cr)_{23}C_6$ transformation during cooling. The more austenite nucleates before A_{c1}, the more carbides precipitate due to the carbon solubility decrease from austenite to ferrite phase. The precipitation of this carbide occurs in α-α grain boundary and grow into α ferrite [7]. Grain coarsening, sensitization from grain boundaries carbides precipitation and martensite formation from the remaining austenite within the ferritic matrix, are the main causes of failure and surface defects among AISI 430 stainless steel [8].

The experimental setup of this research is based on the analysis of the samples listed above (Table 1) by XRD and EBSD. X-ray diffraction (XRD) measurement of each sample kept the rolling direction, where the surface of each specimen was analysed. However, hot-rolled samples were polished with colloidal silica in order to remove roughness from the area of analysis. The 2θ scanning range, step size and count time were 40 - 130°, 0.03º and 2 sec/step, respectively, and Co-Kα radiation (1.79 Á) was used in a Bruker D2Phaser device.

The sample preparation for characterisation by electron backscatter diffraction (EBSD) was carried out with cloth disc and diamond paste auto-polished and a final polishing of colloidal silica suspension. Rolling direction were kept for all the analysis. The EBSD results were acquired by Zeiss Ultra 55 FEG-SEM. Working conditions for the EBSD analysis were: 20 kV voltage and 16.5 mm working distance.

3. Results and discussion

3.1. X-ray diffraction

The phases and their crystalline structures of 1A and 2A ferritic stainless steel were analysed by XRD analysis (Fig. 2). Two manufacturing states were studied, where hot-rolled 1A and 2A correspond to the samples recollected during hot rolling at 1,033 and 920 °C, respectively; besides, annealed 2A specimen was taken after hot rolling and annealing.

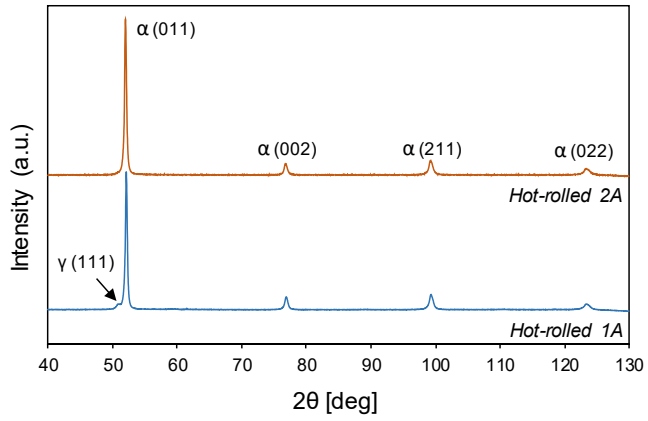

Figure 2. XRD patterns for hot-rolled 1A and 2A ferritic stainless steel.

Results were obtained by Bruker TOPAS based on Rietveld analysis [9]. Diffraction peaks of α (011), (002), (211) and (022) correspond to a ferritic phase. The XRD profile of a hot-rolled 1A shows a ferritic structure, though, a low intensity γ (111) peak is detected near α (011) peak. Besides, 7 % of remaining austenite was measured within the ferritic structure by TOPAS. However, no martensitic could be detected since this phase cannot be distinguished from ferrite via diffraction analysis [10].

Hot-rolled 2A shows an XRD pattern which is in good agreement with ferritic structure. In this case, no visible diffraction for γ (111) peak was detected by TOPAS. The higher ferritic structure of hot-rolled 2A led to increase α (011) peak intensity.

Generally, austenite turns into martensite after quenching when reached Ms temperature. In accordance with *Sung et al.* [7], Ms decreases with increasing Cr_{Eq} and N_2 content in the material composition. Therefore, a non-transformed austenite can be retained within ferrite after fast cooling. This is caused by an exchange of carbon by nitrogen, which promotes atomic ordering of chromium atoms and stabilizes the austenite [10].

This effect of N_2 and Cr_{Eq} on Ms temperature of both specimens, was established using empirical equation for Ms determination. The $\gamma \rightarrow \alpha'$ transformation by cooling is influenced by numerous factors, such as stainless steel composition, grain size, structural defects, etc. Among these, numerous authors [11] considered the stainless steel composition to be the most important.

Eichelman and Hull [9] have developed an empirical equation to calculate Ms temperature. Ms was acquired for both studied materials: $Ms_{(1A)}$: 466 °C; $Ms_{(2A)}$: 487 °C. These results are in good agreement with the previously established around the effect of ferritic stainless steel composition on retention of non-transformed austenite.

Figure 3 shows wide-angle XRD pattern of hot-rolled and annealed 2A ferritic stainless steel series. Annealed 2A diffraction α peaks intensity increased as a result of increasing the ferritic phase of 2A from hot-rolled state to annealed. This points out that the complete transformation of austenite took place during annealing process, and mono-phase ferritic phase was reached after this heat treatment.

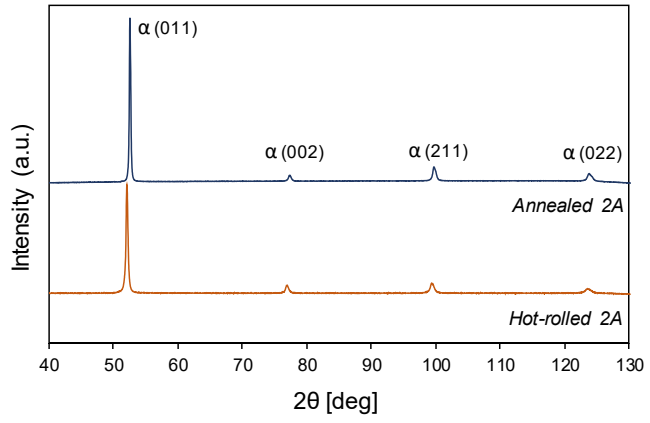

Figure 3. XRD patterns for 2A ferritic stainless steel during hot rolling and after annealing.

3.2. Electron backscatter diffraction (EBSD)

Hot rolling involves not only plastic deformation, but also re-crystallisation happens during this stage, as well as the nucleation of austenite takes place, as it was provided by THERMOCALC in Fig. 1. During the entire hot rolling, both ferritic stainless steels, are in the ferrite - austenite transformation region. From the hot rolling input temperature (Tin_{HR}) to the highest austenite transformation temperature ($T\gamma_{max}$), austenite grows around ferrite grain boundaries, increasing dislocation density, which can prevent ferrite grains from growing [12]. After reaching $T\gamma_{max}$, the reaction is reversed to $\alpha \rightarrow \gamma + M_{23}C_6$ and, therefore, the mechanism around grains growth behaves differently, as will be exposed below.

Figure 4a shows EBSD band contrast (BC) , coincidence site lattice (CSL) and grain boundaries (GB) map of 1A after 87 % of hot rolling reduction at 1,033 °C, where the average aspect ratio is 2.15. CSL and GB allowed identifying sub-nucleation phenomenon of ferrite grains as a result of hot rolling deformation along the normal direction (ND), and re-crystallisation of non-transformed ferrite due to the high temperature of this process. Moreover, BC was also part of this map because it provides a significant contrast difference between ferrite and martensite based on the variation of dislocations and local stress showed by both phases. Equiaxial grains can be observed, while some of them are elongated.

In this specimen, austenite nucleated along the ferrite-ferrite boundaries, which promote the formation of a thin layer of austenite on either side of these boundaries [13]. After quenching, martensite preserved this ordering. EBSD results provided that 70.4 % of the structure was re-crystallised at this point of hot rolling.

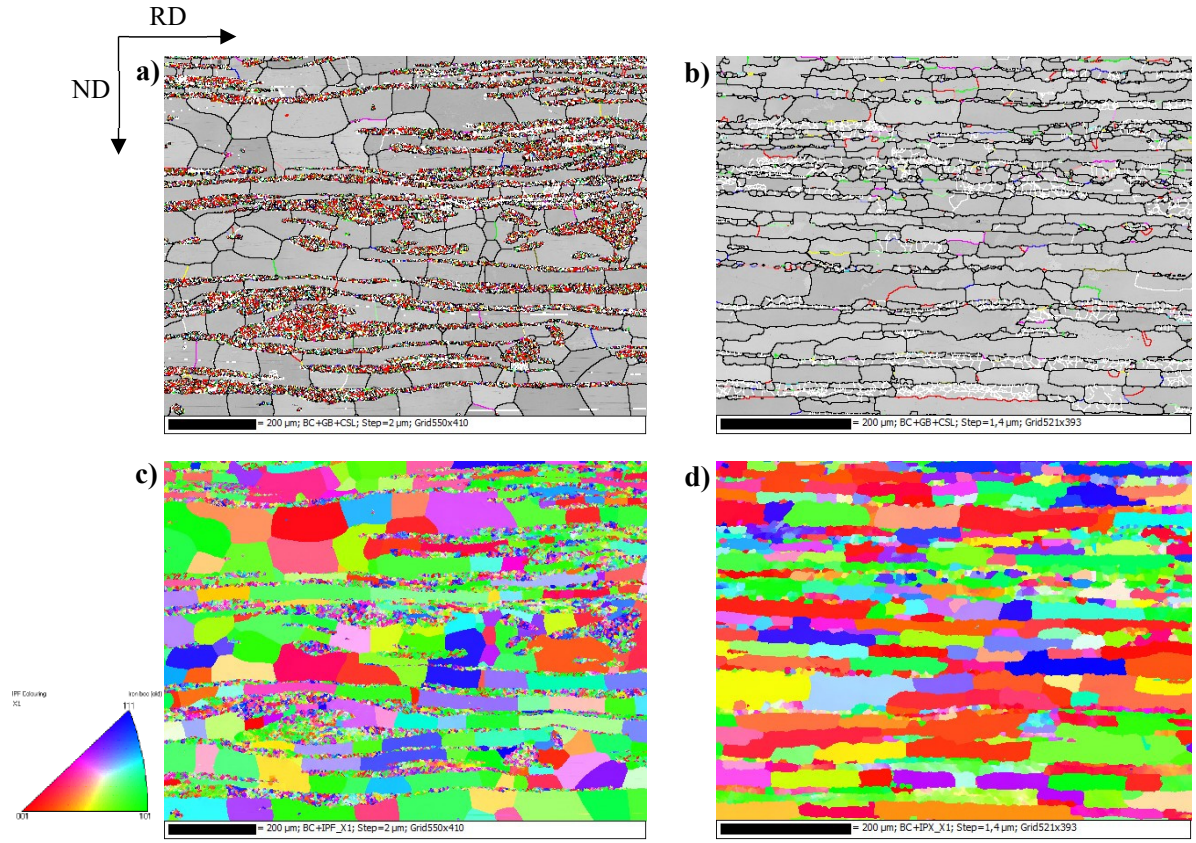

Figure 4. a) Band contrast, grain boundaries and coincidence site lattice (BC+GB+CSL) map; and c) inverse polar figure (IPF) maps of hot-rolled 1A. b) BC+GB+CSL, and d) IPF maps of annealed 1A.

Figure 4b provides annealed 1A BC+CSL+GB map after 98 % of total thickness reduction and initial annealing temperature of 843 °C. It can be observed that coarse grains are mostly elongated along the rolling direction, with an average aspect ratio of 3.27. Furthermore, fine grains are located at coursed grain boundaries; therefore, a wide grain size distribution is reached by 1A. The remained austenite from the previous hot rolling process has completely turned into ferrite and carbides during annealing. Moreover, according to EBSD results, 88.8 % of the structure was recovered after this stage.

Material 2A showed a higher ferritic behaviour during hot rolling than 1A. This performance was a consequence of a change in chemical composition of this alloy, which was based on a higher chromium and lower carbon content, see Fig. 1, leading to a higher Cr_{Eq} of 13.2, compared to 1A specimen. Moreover, as it is shown in Fig. 1, this change in alloy composition led the ferrite - austenite transformation of 2A to be lower than 1A under hot rolling conditions.

The BC+CSL+GB map, displayed in Fig. 5a, shows the 2A structure after 87.1 % reduction at 920 °C. This specimen consisted in both equiaxial and elongated grains, where the average aspect ratio is 2.43. On the other hand, martensite formed within the ferrite structure is thinner and lower in 2A than in the previous hot-rolled 1A sample. These martensite chains were not formed along RD direction since during hot rolling the force is made in the ND plane and some turbulence may occur in the

nucleation of austenite. Therefore, austenite transformation depends not only on the plastic deformation direction during hot rolling, but also on the grain size distribution of the material. In accordance with EBSD analysis, the structure is 80.3 % re-crystallised in this point. This leads to consider that austenitic transformation is the driving force of the re-crystallisation performance of ferritic stainless steel during hot rolling.

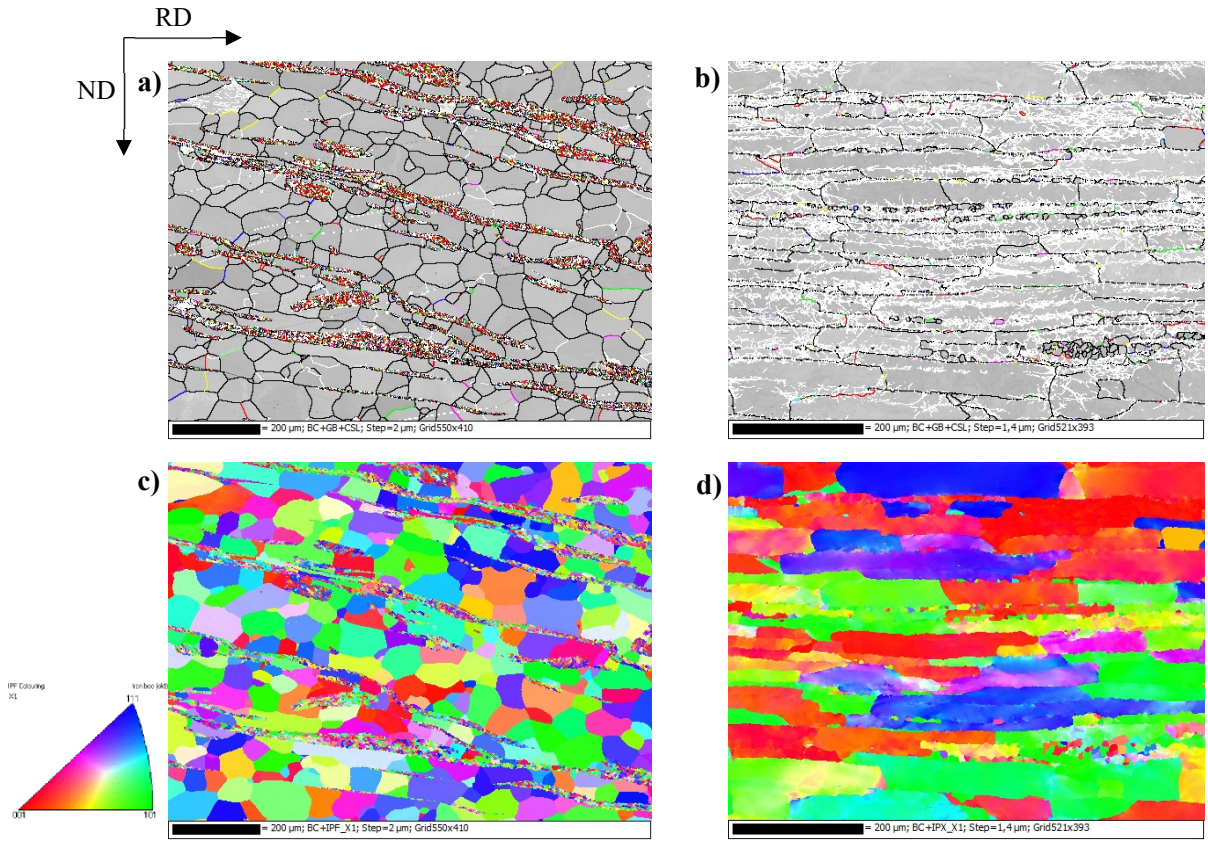

Figure 5. a) Band contrast, grain boundaries and coincidence site lattice (BC+GB+CSL) map; and c) inverse polar figure (IPF) maps of hot-rolled 1A. b) BC+GB+CSL and d) IPF maps of annealed 1A.

Figure 5b shows 2A annealed structure after 98.3 % of total thickness reduction and initial annealing temperature of 826 °C. Coursed grains are highly elongated and showed local stress, see Fig. 5d, which suggests that two considerations must be taken into account. Firstly, in 2A, austenite was rapidly dissolved sufficiently before reaching annealing process. This was due to the amount of austenite transformed during hot rolling was low enough to be completely transformed into ferrite in this stage. Secondly, since the entire annealing energy was invested in the re-crystallisation of mono-phase ferritic structure of 2A, there was an excess of annealing time resulting in excessive ferrite grain growth. This phenomenon during annealing is a common behaviour of ferritic stainless steel type AISI 441 stabilised with Nb and Ti additions to the alloy [14], which prevents the ferrite - austenite transformation at high temperatures, and, therefore, a complete ferritic behaviour is promoted.

EBSD showed that only 3.7 % of the structure was re-crystallised, whereas 56.1 % corresponded to substructure as a result of sub-grains nucleation within coarse ferrite grains, with an average aspect ratio of 2.42.

It is crucial to measure the amount of martensite retained within the ferrite matrix after quenching. This martensite corresponds to the previous austenite transformed at certain temperature during hot rolling. However, martensite and ferrite cannot be discriminated by EBSD so far since their crystal structure are fundamentally equal [15, 16].

For this purpose, a dedicated software (AZTEC RECLASSIFY PHASE [12]) was used in order to quantify that martensite considering EBSP pattern quality parameters. Martensite shows a distorted crystal lattice due to a higher density of crystalline defects, which makes the martensite get a poorer quality, as shown in Fig. 6b, than ferrite phase, shown in Fig. 6a.

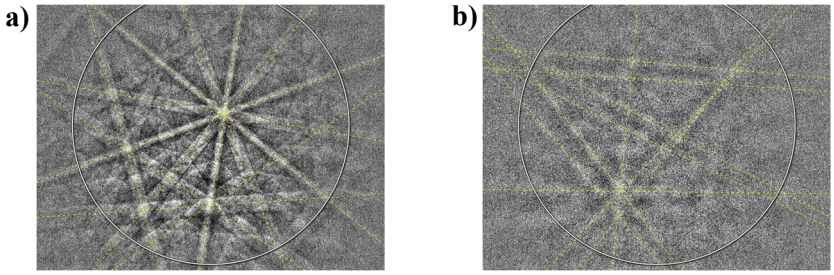

Figure 6. EBSD Kikuchi patterns of a) ferrite and b) martensite obtanined by AZtec Oxford Instruments.

This special feature can be identified by "Band Contrast" (BC) and "Band Slope" (BS) EBSP quality parameters [15], and this is used by the software to identify the martensite areas. Furthermore, these results were checked by non-quantitative conventional light-optical microscopy.

Figure 7 shows BS maps of both AISI 430 studied in this paper during hot rolling, where the martensite (marked in red) is analysed based on its lower pattern quality represented by the darkest areas.

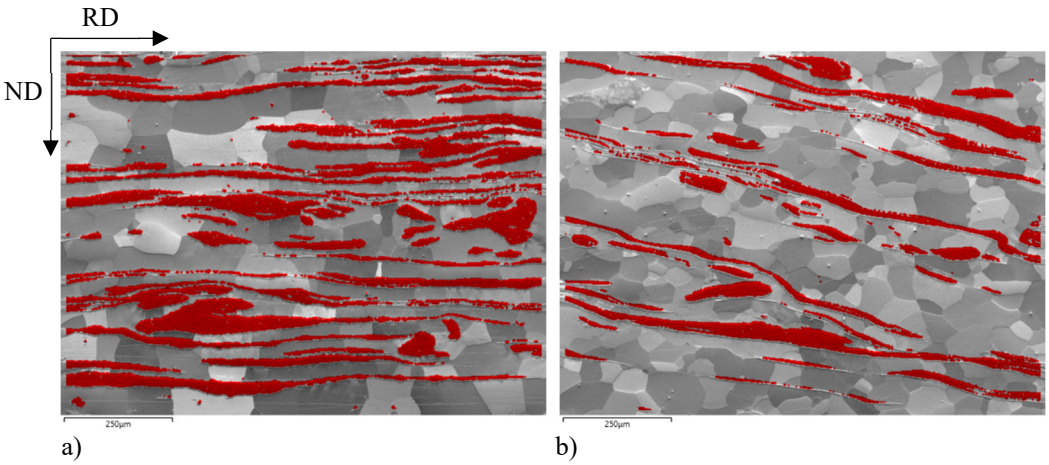

Figure 7. Band slope maps of hot-rolled a) material 1A, and b) material 2A, with martensite reclassified by AZTEC RECLASSIFY PHASE (red areas).

Table 2 lists the remained martensite, quantified by AZTEC RECLASSIFY PHASE, and total deformation of both materials during hot rolling and after annealing, measured by "Recrystallised Fraction" (DefRex) component in Channel 5 HKL. Annealed state of the specimens does not exhibit any retained martensite in the ferrite matrix.

Table 2. Martensite quantified by AZTEC RECLASSIFY PHASE, and deformed fraction of both hot-rolled (HR) and annealed (A) 1A and 2A specimens from EBSD analysis.

ID	State	Martensite, %	Deformation, %
1A	HR	30.8	25.4
	A	0.0	6.2
2A	HR	16.4	15.3
	A	0.0	40.1

3.3. Effect of AISI 430 composition and temperature on microstructure

According to Liu *et al.* [13], the heterogeneous grain-size distribution of both studied materials, during hot rolling and after annealing process, is a consequence of the austenite-ferrite transformation mechanism. A two-stage transformation takes place when the temperature is dropping during hot rolling and the austenite maximum temperature is reached. Therefore, the transformation is inverse from γ to α. The first stage is an interface-controlled reaction, characterised for a fast austenite transformation, which results in large ferrite grains; whereas the second stage leads to small ferrite grains due to slow diffusion-controlled transformation of the austenite [17].

Figure 8a displayed average grain size of both studied materials, where 2A achieved courser average grain size than 1A after the first-stage of hot rolling. Consequently, the austenite transformation in 2A is delayed and slowed down as a result of coarse initial grains and, therefore, the heating rate has a high impact on the phase transformation [18].

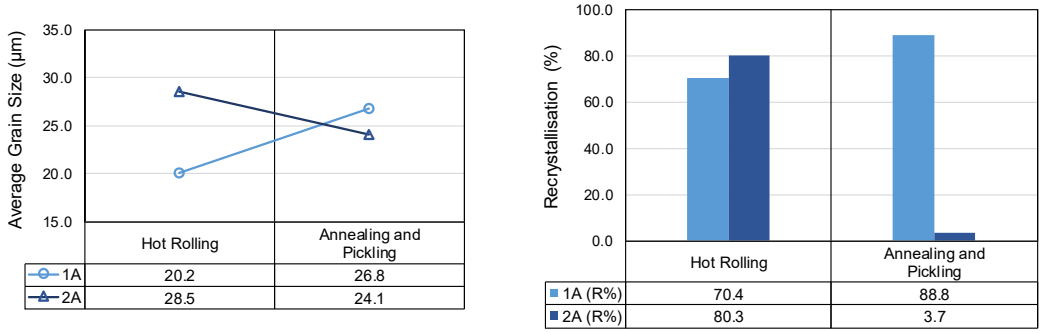

a) b)

Figure 8. a) Average grain size of 1A and 2A during hot rolling and after annealing (EBSD BC+CSL+GB map). b) Re-crystallisation of 1A and 2A during hot rolling and after annealing (EBSD BC+DefRex).

Thickness reduction of 2A during the first-stage of hot rolling was essentially the same as 1A, unlike hot rolling temperature, which was kept lower in 2A. Despite this lower hot rolling temperature, it is

observed in Fig. 8 that 2A structure does not seem to suffer from plastic deformation in terms of grain morphology and re-crystallisation. Material 2A shows an 80.3 % re-crystallised structure (Fig. 8b) at the hot rolling measurement point, versus 70.4 % for material 1A.

Nonetheless, the re-crystallised fraction of 2A dropped after annealing. This leads to point out the importance of cooling rate after hot rolling and annealing time. Despite having retained less austenite than 1A, the cooling time of 2A after hot rolling not only ensured the complete transformation of austenite into ferrite, but also the growth of ferrite grains started to take place. Thus, annealing time was exceeding for this material and, therefore, ferrite grains were elongated and showed a substructure, carried out by sub-grains nucleation.

3.4. Impact of martensite on AISI 430 manufacturing performance

Manufacturing performance of both AISI 430 were evaluated as a function of remaining martensite within ferritic structure. For this purpose, AZTEC RECLASSIFY PHASE was used to measure that martensite fraction.

This investigation is addressed to study microstructural behaviour of flat ferritic stainless steel products. In many occasions, most defects are located at the coil edges; therefore, this work has evaluated microstructural shifts between sheet middle and edges, in order to establish annealing performance in recovering ferritic structure.

Specimens from 1A and 2A sheet middle and edge were taken after both annealing process (annealing and pickling and bright annealing). These samples were analysed by EBSD, where grain size and aspect ratio of the specimens are shown in Fig. 9.

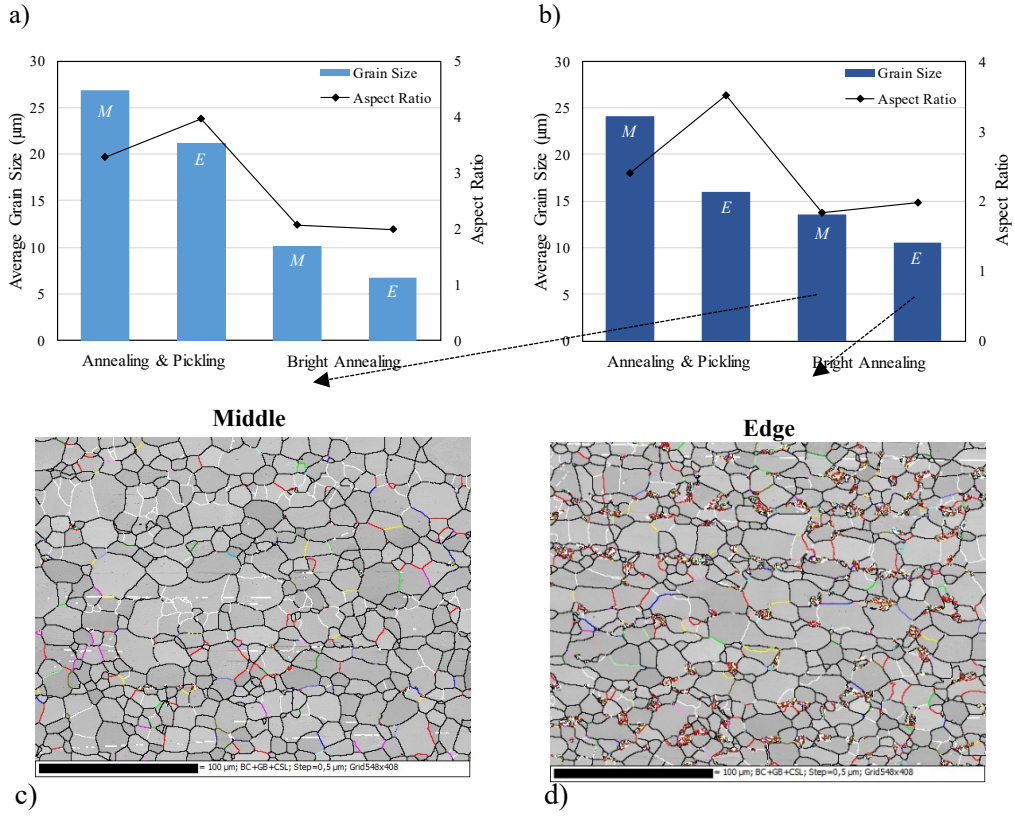

Figure 9. Average grain size and aspect ratio development of annealed a) material 1A, and b) material 2A after annealing and pickling and bright annealing. c-d) EBSD BC+CSL+GB maps of annealed 2A specimens from coil middle and edge after bright annealing (from Fig. 9b).

Re-crystallisation from EBSD analysis and martensite measured by AZTEC RECLASSIFY PHASE for the specimens above are listed in the Table 3.

Table 3. Re-crystallisation and martensite fraction measured by AZTEC RECLASSIFY PHASE of both 1A and 2A specimens collected from sheet middle and edge after annealing processes (annealing and pickling and bright annealing).

AISI 430	Annealing stage	Re-crystallisation %		Martensite %	
		Middle	Edge	Middle	Edge
1A	A&P	88.8	30.6	0	0
	BA	93.3	62.5	5.1	26.3
2A	A&P	3.7	0.7	0	0
	BA	98.2	89.9	0	8.1

These results suggest that the microstructure of 1A and 2A ferritic stainless steel has significantly changed from middle to both edges of each coil because of temperature drop between both points. This different grade of re-crystallisation between the edge and middle site of the coil is also influenced by the geometry of the strip (width) and the energy balance inside the annealing furnace. According to [19], radiation heat transfer is in charge of the over-annealing phenomenon on strip edges.

4. Conclusions

After the last rolling pass, 1A was kept enough time to cool down slowly before reaching the annealing (A&P) temperature. Controlled cooling ensures the $\gamma \rightarrow \alpha + M_{23}C_6$ reaction to partially occur before approaching the annealing stage. During annealing, this material was initially based on ferrite and remaining austenite, and annealing heat led to recover and re-crystallise the ferritic structure (88.8 % R) during cooling from A_{c1} to annealing output temperature.

The aspect ratio of hot-rolled 1A increase after being annealed from 2.15 to 3.27. The coarsening grain was promoted by large cooling time before annealing. Considering that initial microstructure of 1A was based on ferrite and re-crystallisation already started, soak time during annealing caused the coarsening of ferrite grains of annealed 1A.

The 2A cooling range, after the last rolling pass, is shorter than 1A. This means that 2A had less time to complete $\gamma \rightarrow \alpha + M_{23}C_6$ reaction than 1A. Nevertheless, the austenite fraction in 1A is higher than 2A, which can explain that 1A needs slower cooling time than 2A after hot rolling. Despite faster cooling after hot rolling, results have shown that 2A approached annealing process with most of the ferritic structure recovered. Therefore, annealing time should be lower in 2A than 1A, in order to ensure there is not an excess of annealing and subsequent over-growth of grains. According to the aspect ratio of hot-rolled and annealed 2A (2.43 and 2.42, respectively), there is no evidence of grain coarsening phenomenon.

Both 1A and 2A annealed specimens showed a microstructure based on large and small ferrite grains. This heterogeneous grain size distribution depends on austenite to ferrite transformation before A_{c1}, which was promoted by a two-stage reaction controlled by interface and diffusion of austenite transformation, respectively.

Coil middle and edges microstructure of annealed specimens (A&P and BA) were analysed by EBSD and it proved to be an important technique to characterise surface defects related to martensite formation as a result of a temperature shift through the sheet width during annealing controlled by radiative heat transfer inside bright annealing furnace. The site of strip placed by the edges is heated sooner than any site in the middle due to strip geometry and point distance to the furnace interior wall. Furthermore, the

refinement of ferrite grains took place as well as the aspect ratio slightly increase from sheet middle to edges. This indicates that the temperature drop through sheet width generates most surface defects and mechanical failures located in coil edges of AISI 430 ferritic stainless steel.

Acknowledgements
The present work is included in FERRINOP project. Co-funded by CDTI.

References

[1] Núñez A, Llovet X and Almagro J F 2013 Analysis of chemical changes and microstructure characterization during deformation in ferritic stainless steel. *Microsc. Microanal.* **19** 959-968
[2] Ghosh N, Pal P K and Nandi G 2017 GMAW dissimilar welding of AISI 409 ferritic stainless steel to AISI 316L austenitic stainless steel by using AISI 308 filler wire. *Engng. Sci. Tech. Int. J.* **20** 1334-1341
[3] Mehtonen S V, Karjalainen L P and Porter D A 2013 Hot deformation behavior and microstructure evolution of a stabilized high-Cr ferritic stainless steel. *Mater. Sci. Engng. A* **571** 1-12
[4] Vafaeian S, Fattah-alhosseini A, Mazaheri Y and Keshavarz M K 2016 On the study of tensile and strain hardening behavior of a thermomechanically treated ferritic stainless steel. *Mater. Sci. Engng. A* **669** 480-489
[5] Guiraldenq P and Hardouin Duparc O 2017 The genesis of the Schaeffler diagram in the history of stainless steel. *Metall. Res. Technol.* **114** 1-9
[6] Andersson J O, Helander T, Höglund L, Shi P and Sundman B 2002 Thermo-Calc & DICTRA, computational tools for materials science. *Calphad Comput. Coupling Phase Diagrams Thermochem.* **26** 273-312
[7] Ben Rhouma A, Amadou T, Sidhom H and Braham C 2017 Correlation between microstructure and intergranular corrosion behavior of low delta-ferrite content AISI 316L aged in the range 550–700 °C. *J. Alloys Comps* **708** 871-886
[8] Sarkari Khorrami M, Mostafaei M A, Pouraliakbar H and Kokabi A H 2014 Study on microstructure and mechanical characteristics of low-carbon steel and ferritic stainless steel joints. *Mater. Sci. Engng. A* **608** 35-45
[9] Coelho A A (2018) TOPAS and TOPAS-Academic: an optimization program integrating computer algebra and crystallographic objects written in C++. *J. Appl. Crystallogr.* **51** 210-218
[10] Sung J H, Kong J H, Yoo D K, On H Y, Lee D J and Lee H W 2008 Phase changes of the AISI 430 ferritic stainless steels after high-temperature gas nitriding and tempering heat treatment. *Mater. Sci. Engng. A* **489** 38-43
[11] Lo K. H, Shek C H and Lai J K L 2009 Recent developments in stainless steels. *Mater. Sci. Engng. R: Reports* **65** 39-104
[12] Lu H H, Li W Q, Du L Y, Guo H K, Liang W, Zhang W G and Liu Z G 2019 The effects of martensitic transformation and (Fe, Cr) 23 C 6 precipitation on the properties of transformable ferritic stainless steel. *Mater. Sci. Engng. A* **754** 502-511
[13] Haghdadi N, Cizek P, Hodgson P D, Tari V, Rohrer G S and Beladi H 2018 Effect of ferrite-to-austenite phase transformation path on the interface crystallographic character distributions in a duplex stainless steel. *Acta Mater.* **145** 196-209
[14] Sello M P and Stumpf W E 2010 Laves phase embrittlement of the ferritic stainless steel type AISI 441. *Mater. Sci. Engng. A* **527** 5194-5202
[15] Kang J Y, Park S J and Moon M B 2013 Phase analysis on dual-phase steel using band slope of electron backscatter diffraction pattern. *Microsc. Microanal.* **19** 13-16
[16] Nowell M M, Wright S I and Carpenter J O 2009 Differentiating ferrite and martensite in steel microstructures using electron backscatter diffraction. in: *2009 Mater. Sci. Technol. Conf. Exhib. (MS T'09)* **2** 933-943

[17] Liu Y, Wang D, Sommer F and Mittemeijer E J 2008 Isothermal austenite-ferrite transformation of Fe-0.04 at.% C alloy: Dilatometric measurement and kinetic analysis. *Acta Materialia* **56** 3833-3842
[18] Caballero F G, Capdevila C and García de Andrés C 2001 Modelling of Kinetics of Austenite Formation in Steels With different initial microstructures. *ISIJ Int.* **41** 1093-1102
[19] Niederer M, Steinboeck A, Strommer S and Kugi A 2013 Analysis of radiative heat transfer in an indirect-fired strip annealing furnace based on integral equations. *IFAC Proc. Vols.* **46** 403-408